PhD Thesis

PhD Thesis
this is a subtitle

by Oliver Matonoha

LUND
UNIVERSITY

Thesis for the degree of Doctorate
Thesis advisors: Prof. Doktor Professorsson, Prof. Knirk Gnork
Faculty opponent: Prof. Gammal och Grå

To be presented, with the permission of the Faculty of Natural Sciences of Lund University, for public criticism at LINXS (Delta 5, floor 5, IDEON building) on friday, the 30th of October 2023 at 10:15.

Organization	Document name
LUND UNIVERSITY Department of Physics Box 124 SE–221 00 LUND Sweden	**LICENTIATE THESIS** Date of disputation 2020-10-30 Sponsoring organization
Author(s) Oliver Matonoha	

Title and subtitle
PhD Thesis this is a subtitle

Abstract
Lorem ipsum dolor sit amet, consectetuer adipiscing elit. Etiam lobortis facilisis sem. Nullam nec mi et neque pharetra sollicitudin. Praesent imperdiet mi nec ante. Donec ullamcorper, felis non sodales commodo, lectus velit ultrices augue, a dignissim nibh lectus placerat pede. Vivamus nunc nunc, molestie ut, ultricies vel, semper in, velit. Ut porttitor. Praesent in sapien. Lorem ipsum dolor sit amet, consectetuer adipiscing elit. Duis fringilla tristique neque. Sed interdum libero ut metus. Pellentesque placerat. Nam rutrum augue a leo. Morbi sed elit sit amet ante lobortis sollicitudin. Praesent blandit blandit mauris. Praesent lectus tellus, aliquet aliquam, luctus a, egestas a, turpis. Mauris lacinia lorem sit amet ipsum. Nunc quis urna dictum turpis accumsan semper.

Key words
quantum chromodynamics, quark-gluon plasma

Classification system and/or index terms (if any)

Supplementary bibliographical information		Language English
ISSN and key title		ISBN 123456789 (print) 123456789 (pdf)
Recipient's notes	Number of pages 81	Price
	Security classification	

PhD Thesis
this is a subtitle

by Oliver Matonoha

LUND
UNIVERSITY

A licentiate thesis at a university in Sweden takes either the form of a single, cohesive research study (monograph) or a summary of research papers (compilation thesis), which the licentiate student has written alone or together with one or several other author(s).

In the latter case the thesis consists of two parts. An introductory text puts the research work into context and summarizes the main points of the papers. Then, the research publications themselves are reproduced, together with a description of the individual contributions of the authors. The research papers may either have been already published or are manuscripts at various stages (in press, submitted, or in draft).

Cover illustration front: Cool figure by bla and bla.

Cover illustration back: Another cool image by bla.

Funding information: The thesis work was financially supported by the Swedish Research Council.

Faculty of Natural Sciences, Department of Physics

ISBN: 123456789 (print)
ISBN: 123456789 (pdf)

Printed in Sweden by Media-Tryck, Lund University, Lund 2023

Media-Tryck is a Nordic Swan Ecolabel certified provider of printed material. Read more about our environmental work at www.mediatryck.lu.se

MADE IN SWEDEN

Dedicated to
Humpty – Dumpty
bla bla blat

Contents

List of publications

This thesis is based on the following publications, referred to by their Roman numerals:

I **Title paper 1**

S. Doctor, B. Someone
The Journal of Physical Chemistry A, 2020, 124(19), pp. 3943-3946

II **Title paper 2**

S. Doctor, B. Someone, C Another
Physical Chemistry Chemical Physics, 2020, 22(24), pp. 13659-13665

All papers are reproduced with permission of their respective publishers.

Acknowledgements

Lorem ipsum dolor sit amet, consectetuer adipiscing elit. Etiam lobortis facilisis sem. Nullam nec mi et neque pharetra sollicitudin. Praesent imperdiet mi nec ante. Donec ullamcorper, felis non sodales commodo, lectus velit ultrices augue, a dignissim nibh lectus placerat pede. Vivamus nunc nunc, molestie ut, ultricies vel, semper in, velit. Ut porttitor. Praesent in sapien. Lorem ipsum dolor sit amet, consectetuer adipiscing elit. Duis fringilla tristique neque. Sed interdum libero ut metus. Pellentesque placerat. Nam rutrum augue a leo. Morbi sed elit sit amet ante lobortis sollicitudin. Praesent blandit blandit mauris. Praesent lectus tellus, aliquet aliquam, luctus a, egestas a, turpis. Mauris lacinia lorem sit amet ipsum. Nunc quis urna dictum turpis accumsan semper.

Populärvetenskaplig sammanfattning på svenska

Lorem ipsum dolor sit amet, consectetuer adipiscing elit. Etiam lobortis facilisis sem. Nullam nec mi et neque pharetra sollicitudin. Praesent imperdiet mi nec ante. Donec ullamcorper, felis non sodales commodo, lectus velit ultrices augue, a dignissim nibh lectus placerat pede. Vivamus nunc nunc, molestie ut, ultricies vel, semper in, velit. Ut porttitor. Praesent in sapien. Lorem ipsum dolor sit amet, consectetuer adipiscing elit. Duis fringilla tristique neque. Sed interdum libero ut metus. Pellentesque placerat. Nam rutrum augue a leo. Morbi sed elit sit amet ante lobortis sollicitudin. Praesent blandit blandit mauris. Praesent lectus tellus, aliquet aliquam, luctus a, egestas a, turpis. Mauris lacinia lorem sit amet ipsum. Nunc quis urna dictum turpis accumsan semper.

PhD Thesis this is a subtitle

Part I

Fundamental theory

Chapter 1

Introduction to quantum chromodynamics

1.1 Standard Model of elementary particles

One paragraph QFT
One paragraph description
One paragraph successess and drawbacks

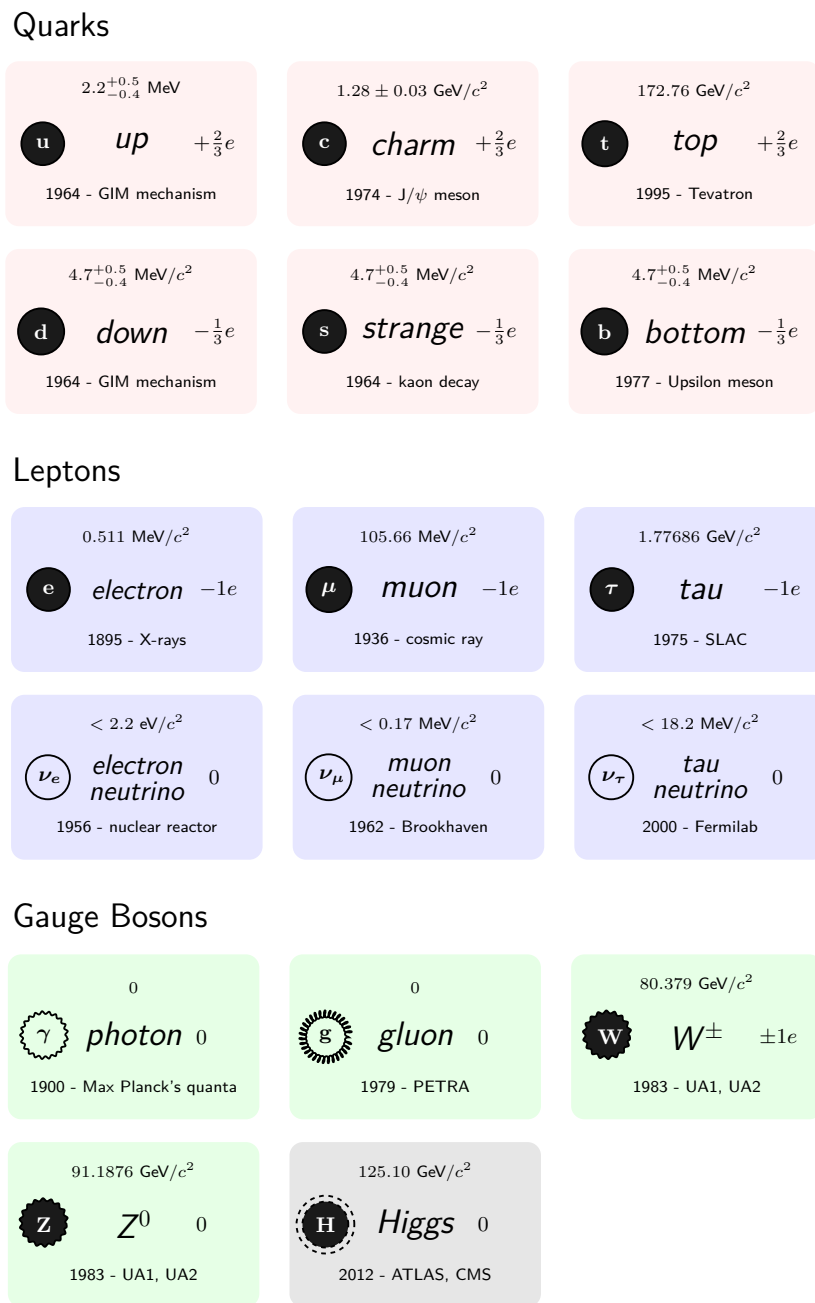

Figure 1.1: Standard model.

1.1.1 Quantum Electrodynamics

One paragraph

1.2 Coordinate systems and kinematic observables

Particles in HEP processes are described by their Lorentz-invariant four-vectors, $\boldsymbol{x} = (ct, x, y, z)$ and $\boldsymbol{p} = (E/c, p_x, p_y, p_z) = (E/c, p_\mathrm{T}, p_z)$. In LHC experiments, the coordinate system is defined such that the x-axis points in the direction of the LHC, and the z-axis points in the direction of the beam, as shown in Fig. 1.2. In addition to the standard Cartesian coordinates, two observables, φ (azimuthal angle) and η (pseudorapidity), are used to describe the position and momentum of particles relative to the interaction point, which is located at $x = y = z = 0$. Pseudorapidity is defined as a function of the polar angle θ, where

$$\eta = -\ln(\tan(\theta/2)) \quad . \tag{1.1}$$

For high-momentum particles ($p \geq mc$), pseudorapidity is an approximation of the rapidity relative to the beam, given by

$$y = \frac{1}{2} \ln \frac{E + p_z c}{E - p_z c} \quad . \tag{1.2}$$

Rapidity is a convenient quantity to use because it transforms additively under Lorentz boosts, unlike velocity. In these coordinates, the following relations hold:

$$p_x = |\vec{p_\mathrm{T}}| \cos\varphi \,, \qquad p_y = |\vec{p_\mathrm{T}}| \sin\varphi \,, \qquad p_z = |\vec{p}| \sinh\eta \,. \tag{1.3}$$

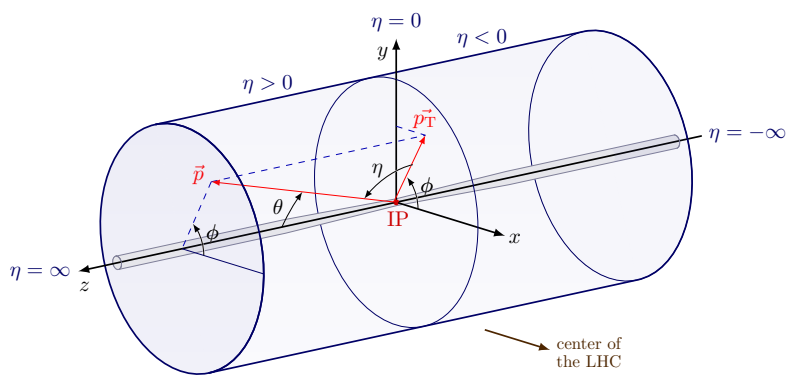

Figure 1.2: Coordinate system of an LHC experiment.

1.3 Processes involving gluons

Diagrams, screening(?), divergences

1.3.1 Running coupling constant

One paragraph, one figure

1.3.2 Perturbative QCD

One paragraph

1.4 From partons to hadrons

1.4.1 Initial and Final State Radiation

In quantum field theory, charged particles are surrounded by a cloud of virtual particles, which can be thought of as fluctuations in the particle's field. For example, the electron state can be described as a superposition of the bare electron plus additional massless bosons:

$$|\mathrm{e}\rangle_{\mathrm{phys}} = |\mathrm{e}\rangle + |\mathrm{e}\gamma\rangle + |\mathrm{e}\gamma\gamma\rangle + \ldots \tag{1.4}$$

and, at higher orders, pairs of virtual electrons. The fluctuations continuously form and recombine, with their lifetime depending on their energy and momentum. Specifically, the lifetime of a fluctuation with energy ω and transverse momentum k_{T} can be approximated as:

$$\tau \approx \frac{\omega}{k_{\mathrm{T}}} \quad . \tag{1.5}$$

This implies that fluctuations with smaller-k_{T} live longer.

As illustrated in Fig. 1.3, the coherent mixed state of the bare charge and the field fluctuations can be disturbed by the presence of an interaction. Intuitively, this interaction can change the energy and momentum of the fluctuations, their formation and recombination, and lead to the emission of radiation in two ways:

1. a fluctuation is kicked on-shell by the interaction and part of the field continues in its original direction, which leads to Initial State Radiation (ISR);

2. as a result of the field of the scattered particle rearranging itself , which can be a source of Final State Radiation (FSR).

In both of the cases, a larger momentum transfer implies more radiation. *For hard, wide angle emissions, cross sections can be calculated perturbatively at fixed orders.*

Soft and collinear emissions, however, lead to infra-red divergences ($\propto \frac{1}{\omega}$,$\propto \frac{1}{k_{\mathrm{T}}^2}$) and thus, need to be factorised away from the amplitudes or the cross sections and then described using resummation techniques. Without any emissions, the probabilities of finding electrons and photons of fractional momentum x with respect to the whole system are:

$$f_{\mathrm{e}}(x) = \delta(1-x)\,, \qquad f_{\gamma}(x) = 0\,, \tag{1.6}$$

When considering the emissions above some scales parametrised by the resolution parameter Q^2, these probabilities, however, evolve according to the DGLAP equation:

$$\frac{\partial}{\partial \ln Q^2}\begin{pmatrix} f_e(x,Q^2) \\ f_\gamma(x,Q^2)\end{pmatrix} = \frac{\alpha_{\mathrm{em}}}{2\pi}\int_x^1 \frac{dz}{z}\begin{pmatrix} P_{ee}(z) & P_{e\gamma}(z) \\ P_{\gamma e}(z) & P_{\gamma\gamma}(z)\end{pmatrix}\begin{pmatrix} f_e\left(\frac{x}{z},Q^2\right) \\ f_\gamma\left(\frac{x}{z},Q^2\right)\end{pmatrix}\,, \tag{1.7}$$

where $P_{ij}(z)$ are the splitting probability functions of a particle i emitting a particle j.

In QCD, the behaviour is analogous, with $\alpha_{\mathrm{em}} \to \alpha_s$, $e \to q$, and $\gamma \to g$.

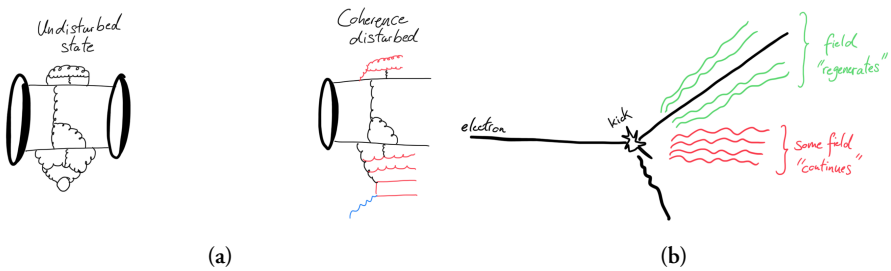

Figure 1.3: Illustration of the field fluctuations and emmisions of radiation in a scattering process.

1.4.2 Factorisation theorem

The evolution equations 1.7 imply that the probabilities of observing emissions with a fractional momentum x depend on the resolution Q^2. In QCD,

1. when applied to the initial state, they are known as parton distribution functions (PDFs) and determine the probabilities of finding partons[1] in the composite hadronic state.

2. When applied to the final state, they are called fragmentation functions, and determine the probabilities of measuring fragments of the outgoing particles.

This leads to the factorisation theorem for processes involving collisions of two hadrons, which separates the perturbatively calculable partonic cross section from the non-perturbative partonic evolution and hadronisation. The theorem can be expressed as follows:

$$\sigma = f_i^A(x_i, \mu_F) f_j^B(x_j, \mu_F) \otimes \hat{\sigma}_{ij\to n}(\mu_F, \mu_R) \otimes D_{n\to n'} \,. \tag{1.8}$$

Here, i and j are the initial partons, $\hat{\sigma}_{ij\to n}$ is the partonic cross section, $D_{n\to n'}$ is the process-specific fragmentation function for evolving the partons n into the particles' final state n', and μ_F and μ_R are the factorisation and renormalisation scales, respectively. The factorisation scale, μ_F, determines the scale below which the emissions are absorbed into the PDFs. The theorem is depicted in Fig. 1.4.

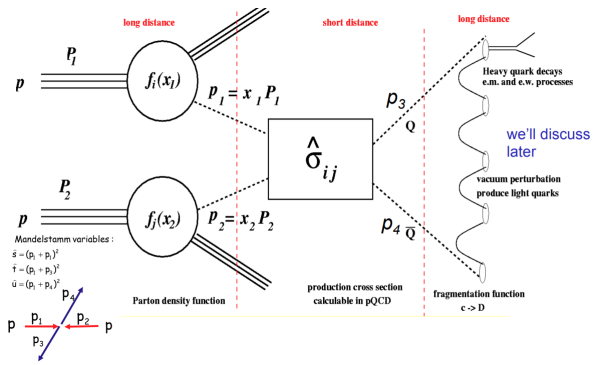

Figure 1.4: Illustration of the factorisation theorem. (NEEDS TO BE REMADE).

1.4.3 Parton distribution functions

The PDFs defining the probabilities of finding quarks and gluons in nucleons can be determined experimentally at hadron-electron colliders such as HERA. They are determined from measurements of deep inelastic scatterings in a range of energies and momentum transfers. They are displayed in Fig. 1.5 as a function of the fractional momentum x (also called Björken x).

[1]Partons refer to the valence quarks, sea quarks, and gluons inside hadrons.

According to collider kinematics, $x \propto \frac{1}{\sqrt{s}}$, therefore, the partonic composition of ultra-relativistic hadrons is dominated by gluons. Following unitarity principles and BK evolution equation, it is expected that gluons start recombining and the gluonic content saturates as $x \to 0$. This is actively reseached, however, not directly measured yet. Additionally, it should be noted that in ultra-relativistic heavy nuclei, the partons are modified in the contracted nuclear environment and the PDFs are referred to as nPDFs.

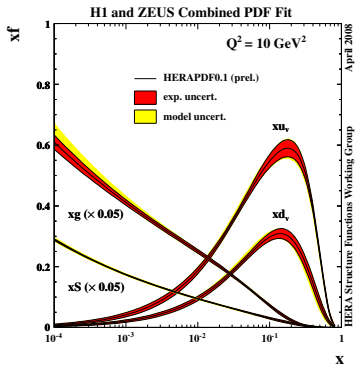

Figure 1.5: Parton distribution functions determined at HERA. TBA

1.4.4 Parton fragmentation and the Lund string

After the scattering process, the produced partons continue to fragment by emitting more partons in a process called the parton shower. Since the coupling strength in QCD increases with decreasing the energy scale of the splitting, this leads to the production of many soft, collimated emissions known as jets. The partonic evolution continues until the virtuality of the partons reaches the hadronization scale ($\approx \Lambda_{\mathrm{QCD}}$). There are multiple frameworks within QCD to describe the evolution of partons into their final state, such as using the DGLAP equations or the so-called dipole formalism.

Once the partonic final state is reached, the partons hadronise into the observable mesons and baryons. The hadronisation process is not calculable in QCD and requires phenomenological models to describe it. One such model is the Lund String model, which describes hadronisation as the breaking of a color string between the quarks in the final state. In this model, the energy stored in the color string is converted into the mass of new hadrons.

According to confinement, hadronisation should involve at least two partons with

complementary colours. In QCD, the $q\bar{q}$ potential takes the shape of

$$V_{q\bar{q}} \approx -\frac{4}{3}\frac{\alpha_s \hbar c}{r} + \kappa r \quad , \tag{1.9}$$

where κ is a paramater with value around $1\mathrm{GeV/fm}$. In the non-perturbative regime (long distances), the potential is dominated by the linear part, which is reminiscent of a system bound by a string with tension κ. This is taken advantage of by the Lund string model – a q and $\bar{q}$ pair separated by distance Δx is bound by a color field (string) with energy $\kappa \Delta x$.

If the q and $\bar{q}$ continue separating as a result of the scattering, the energy stored in the color field increases. At some point, it can become energetically favourable to produce a new $q\bar{q}$ pair out of vacuum, which is a quantum mechanics tunnelling phenomenon characterised by the probability:

$$\frac{\mathrm{d}P}{\mathrm{d}m_\mathrm{T}} \propto \exp\left(-\frac{\pi m_\mathrm{T}^2}{\kappa}\right) \quad , \tag{1.10}$$

where m_T is the transverse mass of the produced quarks. Otherwise, the $q\bar{q}$ system starts contracting and oscillates with a period $T = 2E_\mathrm{kin}/\kappa$, where E_kin is its maximum kinetic energy. The produced q and $\bar{q}$ then connect by new color fields to the original pair. This process repeats itself result in cascade of many $q\bar{q}$ pair connected by many color strings. In this descriptions, baryons can also be created by double tunnelling of a $qq\bar{q}\bar{q}$ pair. The process is illustrated in Fig. ??.

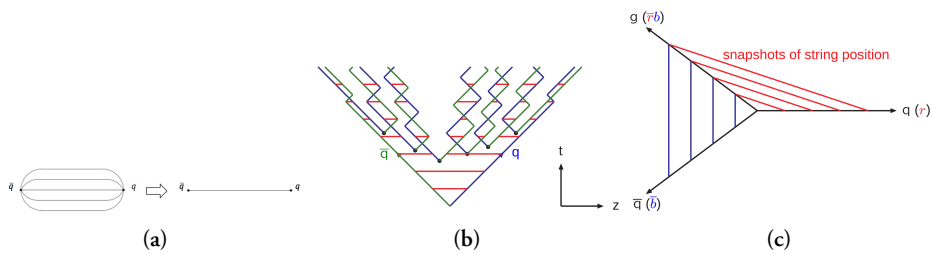

Figure 1.6: Illustration of the color field between two quarks and its simplified representation with a string. Illustration of the string splitting by producing new $q\bar{q}$ in the $t-z$ plane. Illustration of the treatment of gluons in the Lund string model.

Equation 1.10 also implies that production of strange quarks is suppressed by a factor of

$$\rho = \exp\left(-\frac{\pi(m_s^2 - m_{u,d}^2)}{\kappa}\right) \quad . \tag{1.11}$$

This parameter is typically tuned to data, as substituting constituent ($m_s \approx 0.5\,\mathrm{GeV}/c^2$, $m_{u,d} \approx 0.33\,\mathrm{GeV}/c^2$) versus current masses ($m_s \approx 0.1\,\mathrm{GeV}/c^2$, $m_{u,d} \approx 0$) leads to considerable differences underestimating and overestimating data, respectively.

For a $q\bar{q}g$ system, in this model, the gluon connects to the quark and antiquark and is effectively treated as a "kink" on the color field, adding energy and momentum to the $q\bar{q}$ string (stretching it in its direction), as visualised in Fig. **??**.

It should be noted that in the paradigm of AA collisions, hadron production can be alternatively modelled by hadronisation at the QGP's phase boundary by *coalescing* free quarks.

TBA a sentence about the actual hadronisation.

1.5 Lattice QCD

One paragraph

1.6 QCD phase diagram

One paragraph, figure

1.6.1 Phase transition

One paragraph, bag model derivation of T

1.6.2 Chiral symmetry restoration

One paragraph, figure

1.7 Implications

One paragraph

Chapter 2

QCD phenomena in high energy hadronic collisions

2.1 Collisions of heavy nuclei

2.1.1 Collision geometry, Centrality, multiplicity

Collisions of heavy nuclei, composed of many fluctuating nucleons, may occur under various initial state configurations. Some quantities used to describe them are the impact parameter b, defined as the distance between the two nuclei centers, number of participating (scattered) nucleons N_{part}, and the number of binary nucleonic collisions N_{coll}.

Determining these quantities is important because:

1. Soft processes, such as light flavor particle production, are expected to scale with the interaction volume, which $\propto N_{\mathrm{part}}$.
2. Hard processes, such as jet and heavy flavor production, are expected to scale with the number of large momentum transfer interactions given by N_{coll}.
3. b, disregarding the fluctuations of nucleonic positions, defines the shape and anisotropy of the overlap region, which are important initial state conditions.

Since these quantities cannot be directly measured, they need to be modelled. The charged particle *multiplicity* is commonly used for this purpose, as $\langle N_{\mathrm{ch}} \rangle$ increases

monotonically with N_{part}, N_{coll}, and decreasing b. Multiplicity N_{ch} can be measured experimentally, e.g. with tracking detectors. The concept of *centrality* is also used, which is defined as quantiles of the total nuclear cross-section. For example, a centrality of $0-5\%$ refers to low b values and the top 5% of N_{ch} values (central events), while $95-100\%$ centrality refers to high b values and the bottom 5% of N_{ch} values (peripheral events). Centrality can also be inferred from other *event activity* classifiers, such as amplitudes of scintillators at forward rapidity, transverse energy in calorimeters, or energy from beam remnants in zero-degree-calorimeters.

In AA collisions, these relationships are well-defined, and thus the models perform well. The most popular model is the MC Glauber model. Other models include MC-KLN and IP Glasma.

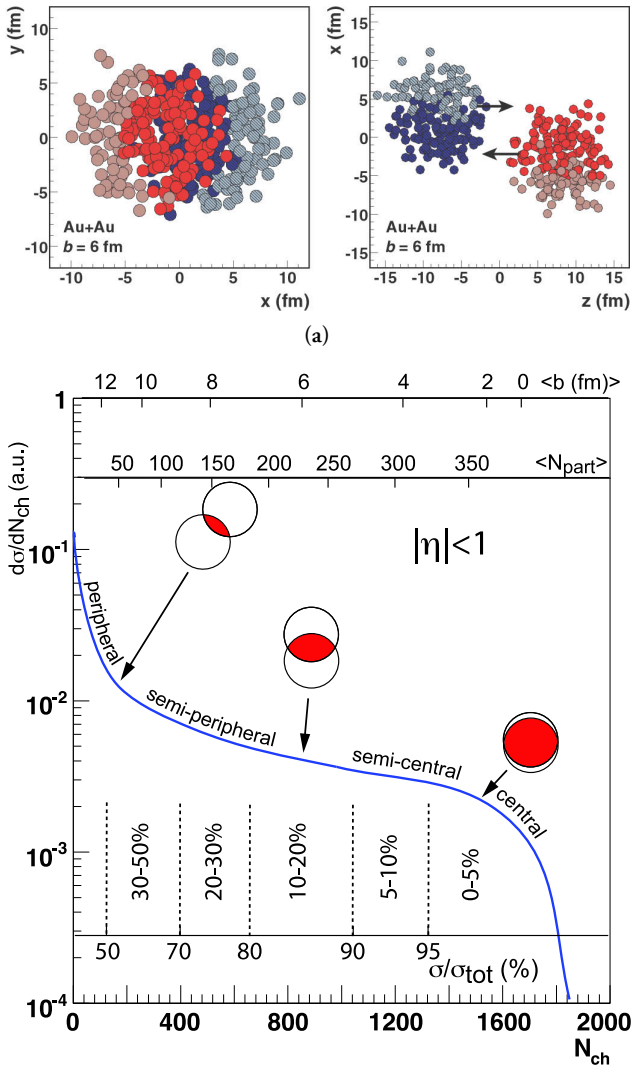

Figure 2.1: TBA

2.1.2 MC Glauber model

The MC Glauber model takes on a very simple albeit powerful approach. The two nuclei are simulated in three dimensions in a way that satisfies their respective nuclear density profiles, usually modelled by sampling the positions of nucleons from the Wood-Saxon distribution:

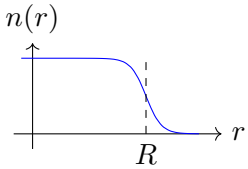

$$n(r) = \frac{1}{1 + \exp((r - R)/a)} \quad , \quad (2.1)$$

where R is the nuclear radius and a the nuclear skin thickness.

The nucleonic densities can be represented by uniform disks, or more accurately by Fermi-distributions or Gaussian profiles to account for fluctuations of their densities. Their parameters are left free and are tuned to the data.

A random impact parameter is then chosen or sampled. The collision is then treated as a sequence of independent binary nucleon-nucleon collisions, where

1. nucleons remain travelling in straight lines,
2. the inelastic nucleon-nucleon cross section σ_{NN} does not depend on the number of interactions,
3. two nucleons are considered to interact if their transverse relative distance $d \leq \sqrt{\sigma_{\mathrm{NN}}/\pi}$.

Fig. 2.1 illustrates an example of a Glauber Monte Carlo event for a Au+Au collision. By simulating numerous collisions, the average N_{part} and N_{coll} are determined[1], and their relations to centrality and event activity observables are determined by fitting to experimental data.

Recent studies have extended the MC Glauber model to include sub-nucleonic structures. Such efforts show that the production of charged hadrons at mid-rapidity scales linearly with the number of participating partons. Comparisons with LHC data at $\sqrt{s_{\mathrm{NN}}} = 5.02\,\mathrm{TeV}$ suggest that the number of sub-nucleonic degrees of freedom ranges from 3 to 5? .

2.2 Quark-gluon plasma

In agreement with lattice QCD predictions, the QGP has been measured in ultra-relativistic collisions of heavy nuclei at RHIC? , LHC? , and even SPS? . Although it

[1]It also shows the scaling between the numbers of participants and binary collisions, which is approximately $N_{\mathrm{coll}} \approx 0.35 N_{\mathrm{part}}^{4/3}$.

cannot be observed directly, a wealth of evidence from three decades of research combining various observables reveals the effects of the produced QGP medium. Whilst somewhat context-dependent, the following features make QGP the most extreme phenomena observed phenomena in terms of its:

- *Temperature*: QGP temperatures reach values on the order of hundreds of MeV, which corresponds to approximately 2×10^{12} K.[2]
- *Viscosity*: the shear viscosity to entropy density ratio η/s reaches the minimum quantum limits of $1/4\pi$, making it an almost perfect liquid.
- *Vorticity*: in semi-peripheral collisions, the rotating plasma reaches a vorticity parameter of approximately 0.4 fm^{-1}.
- *Magnetic field*: in non-central collisions, the magnetic fields of the heavy nuclei may peak at $\sim 10^{19}$ T.

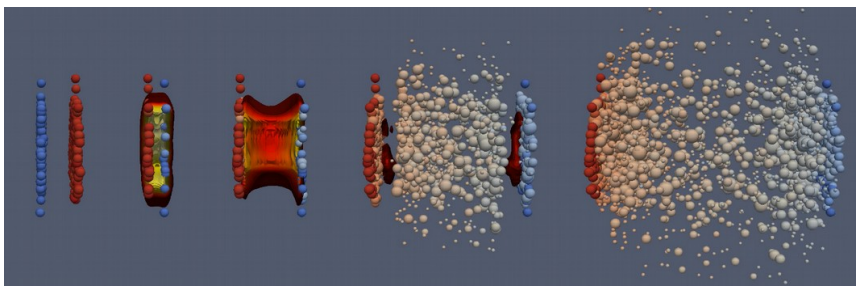

Figure 2.2: TBA

Figure 2.2 illustrates the mainstream paradigm of a heavy nuclei collisions evolution:

1. The Lorentz-contracted heavy nuclei approach each other at ultra-relativistic speeds.
2. *Pre-hydrodynamisation stage* ($\tau \equiv \sqrt{t^2 - z^2} \leq 1$ fm/c): "hard" particles are produced in scatterings with the highest momentum transfer Q^2, produced matter expands rapidly in longitudinal directions and starts expanding in radial direction.
3. *Hydrodynamisation* ($1 \leq \tau \leq 10$ fm/c): partons are abundantly produced, creating a deconfining medium and allowing the system to be described by hydrodynamic equations.

[2]Contrasting some of the lowest temperatures required for the super-conducting magnets of the LHC, $T \approx 1.9$ K.

4. *Chemical freeze-out* ($\tau \sim 20$ fm/c): the cools down, hadronises, produced hadrons then stop interacting inelastically and the system's chemical content is stabilised.

5. *Thermal freeze-out*: hadrons no longer interact elastically and their kinematics stabilize.

The following subsections outline some of the essential phenomena related to the production of QGP.

2.2.1 Quarkonium dissociation and sequential suppression

Heavy quarkonia are vector mesons of $c\bar{c}$ and $b\bar{b}$. They include J/ψ, $\psi(2S)$, $\Upsilon(1S)$, $\Upsilon(2S)$, $\Upsilon(3S)$, which can be relatively easily measured in LHC experiments via their di-lepton decay channels. They are created solely in the first phases of the collision and then experience the entire evolution of the QGP medium:

$$t^{Q\overline{Q}}_{\text{creation}} < t^{\text{QGP}}_{\text{creation}} < t^{\text{QGP}}_{\text{lifetime}} \ll t^{Q\overline{Q}}_{\text{lifetime}} \quad . \tag{2.2}$$

Additionally, due to their large binding energies, their radii may remain smaller than the plasma screening radius $r_{\text{D}}(T)$, and thus, survive the dissociation. For instance, considering their in-vacuum radii determined from the $q\bar{q}$ potential, $r_{\Upsilon(1S)} \sim 0.14$ fm, $r_{\Upsilon(2S)} \sim 0.28$ fm, $r_{\Upsilon(3S)} \sim 0.39$ fm, which contrast the $r_{\pi} \sim 0.7$ fm. This implies that different temperatures result in the dissociation of different states, and measuring the production of different states can help infer QGP temperature, as illustrated in Fig. 2.3.

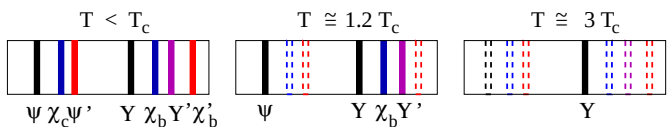

Figure 2.3: TBA

The production of heavy quarkonia in AA collisions is compared to that in pp collisions through the nuclear modification factor, R_{AA}. This factor is widely used in various other AA measurements and is defined as:

$$R_{\text{AA}} = \frac{\mathrm{d}N_{\text{AA}}/\mathrm{d}p_{\text{T}}}{\langle N_{\text{coll}} \rangle \, \mathrm{d}N_{\text{pp}}/\mathrm{d}p_{\text{T}}} \quad . \tag{2.3}$$

R_{AA} can take on the following values:

1. $R_{\mathrm{AA}} = 1$: There is no net effect on the production, corresponding to the absence of the QGP medium and other nuclear effects.

2. $R_{\mathrm{AA}} < 1$: The production is overall suppressed, for example, due to dissociation.

3. $R_{\mathrm{AA}} > 1$: The plasma and nuclear effects systematically enhance the measured production.

At LHC energies, the abundance of charm quarks in the QGP is high enough that charmonia can be reformed after dissociation, which somewhat complicates the interpretation of their suppression. However, the $\Upsilon(3S)$ bottomonium has R_{AA} consistent with 0 at $\sqrt{s_{\mathrm{NN}}} = 5.02$ TeV, as shown in Figure 2.4. This complete suppression is a clear signature of the QGP and can be used together with models to estimate the QGP temperature at these energies as $T \approx 630$ MeV.

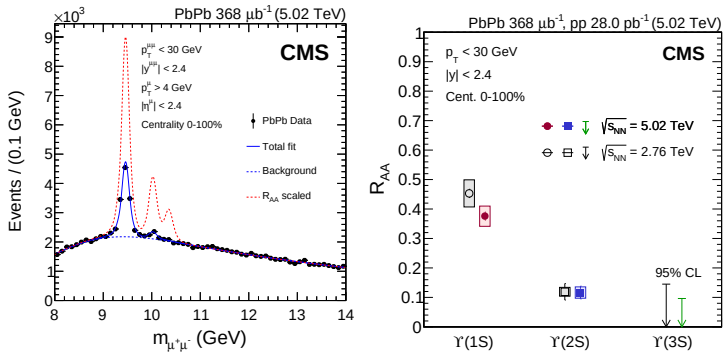

(a) (b)

Figure 2.4: TBA

2.2.2 Strangeness enhancement

TBA

2.2.3 Collective flow

TBA

2.2.4 Jet quenching

TBA

2.2.5 Cold nuclear matter effects

It should be noted that apart from the QGP, other effects come into play due to the fact that the collision involves two nuclei instead of two protons. These effects are important caveats to bear in mind and include:

1. Nuclear (anti-)shadowing: Reflects the modification in production due to differences in nPDFs and PDFs.
2. Cronin effect: Describes the initial parton energy loss due to scatterings in the nuclear medium and broadens measured p_{T} spectra.
3. Nuclear absorption: Describes the dissociation of particles due to their interactions with the passing-by nuclear remnants. It is generally negligible at LHC energies.
4. Co-mover absorption: This is the effect of inelastic interactions with the hadron gas.

These effects can be isolated and quantified in pA or very peripheral AA collisions.

2.3 QGP phenomena in small systems

Measurements within the last decade have shown that certain QGP phenomena can also be observed in high-multiplicity events of pp collisions at LHC energies, which challenges the traditional assumption that QGP is only produced in AA collisions. This has sparked debates about the existence of QGP in pp collisions and, to a lesser degree, about the absence of QGP in AA collisions, despite the extensive experimental evidence.

Furthermore, the observed behavior of these phenomena indicates that the role of event multiplicity N_{ch} may be more significant than system size. This has led to ongoing efforts to establish a consistent and seamless link between the paradigms of pp and AA collisions.

Strangeness and charm enhancement

ALICE measurements on Λ/π, Ξ/π, and Ω/π ratios demonstrate that the production rates of particles containing strange quarks increase faster with multiplicity than those containing only u and d quarks. This also depends on the strangeness content – the effect is the strongest for Ω and vanishes for protons. Furthermore, the evolution to larger systems seems to be continuous with respect to N_{ch}. The measurements can be seen in Fig. 2.5.

To contrast the strangeness measurements with heavier flavour, the $J/\psi\ /\pi$ ratio also shows a clear increase in yield with increasing N_{ch} in pp collisions, as is shown in Fig. 2.5. However, this comes with an important caveat: high-multiplicity events are biased to have enhanced hard processes, as discussed further in Chapter X. Moreover, the evolution of this phenomenon is also not continuous with N_{ch} when going from pp collisions at $\sqrt{s} = 13\,\mathrm{TeV}$ to $\sqrt{s_{\mathrm{NN}}} = 5.02\,\mathrm{TeV}$, which can also be explained by the fact that charm quarks are produced solely in hard scattering processes, the rates of which depend on the collision system and center-of-mass energy.

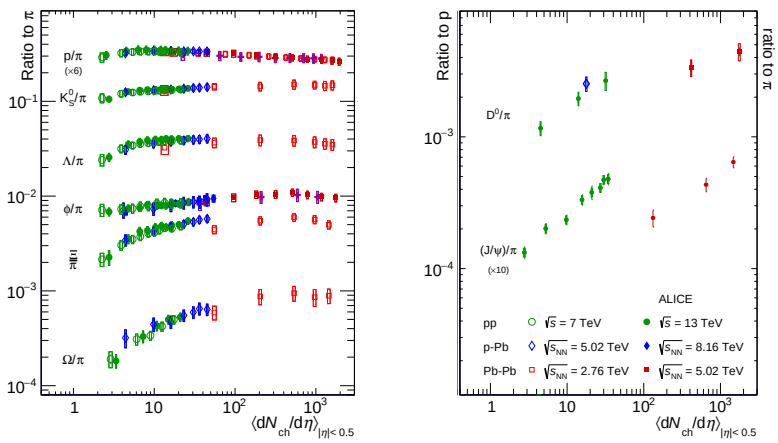

Figure 2.5: TBA

Anisotropic flow

Measurements of azimuthal correlations and anisotropic flow in small collision systems exhibit features of a collectively expanding system, similar to those observed in heavy-ion collisions, where they are believed to originate from the presence of QGP medium. The origin of the collective effects depends on particle multiplicity of a collision. While hydrodynamic-like description seems to be favored by data especially

at high multiplicities, the effects of initial state effects from initial gluon momentum correlations may play an important role at low-Nch.

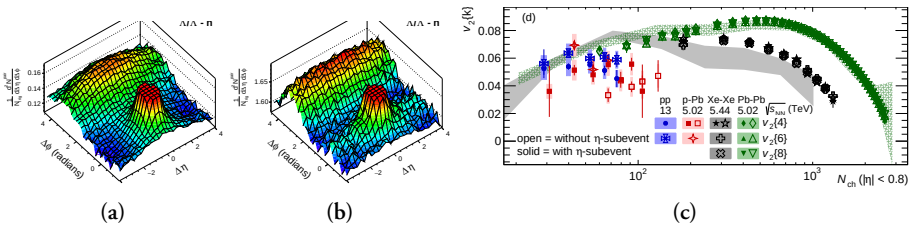

Figure 2.6: TBA

Radial flow

the ratio between ☒ and Ko S pT spectra was measured in pp interactions characterised by different final-state multiplicities [844]. The idea behind this observable is that the radial boost of a collectively-expanding system should impact the heavier hadrons more strongly, giving rise to the observation of an enhanced baryon-to-meson ratio at intermediate-pT. This enhancement is observed in the ☒/K o S ratio for small collision systems in a qualitatively very similar way as in heavy-ion interactions. The magnitude of the intermediate-pT enhancement increases as the multiplicity increases and the peak position moves towards higher values for high-multiplicity collisions, in agreement with the hydrodynamic origin picture. Moreover, the increase at intermediate momenta is accompanied by a corresponding depletion of the ratio at low-momenta, with the integrated ☒/K o S ratio exhibiting essentially no multiplicity dependence in pp collisions. This observation also holds for proton-to-pion ratios and is qualitatively reminiscent of what is observed in Pb–Pb collisions, as described in Sec. 2.3.2. In order to study the low-pT depletion and mid-pT enhancement more quantitatively, specific pT regions have been selected and the multiplicity dependence of the ☒/K o S ratio in these intervals is reported in the right panel of Fig. 82. Similar studies have also been carried out recently for the charmed baryon-to-meson ratio ☒c/D o , where similar behaviour has been observed [837]. The corresponding results are shown in Fig. 82 together with the ☒/K o S ratio and exhibit a pattern consistent with the non-charmed baryon-to-meson ratio, although future measurements with smaller uncertainties are still needed to come to a firm conclusion.

Sequential suppression of Y states

Including analysis of event geometry via spherocity, which suggests effect is connected with UE not jets

As event multiplicity (should be UE) grows larger, excited ⊠ states are, compared to the ground state, relatively less likely to be found

Is it even a suppression? Maybe it's a lower state enhancement? àIn any case seems to be a hard – UE correlated phenomenon

Seems we don't understand Upsilon hadronization as it depends on the UE

Furthermore, if we consider only the events with 0 < ST < 0.55, where none or little dependence on multiplicity is present, the mean number of charged particles per event is ex- actly the same for the three ⊠ states (⊠Ntrack ⊠ = 22.4 ± 0.1). This suggests that the different number of associated particles is not directly linked to the difference in mass between the three states.

Important caveat here is that the hadronic decay of upsilon may result in tens of produced hadrons.

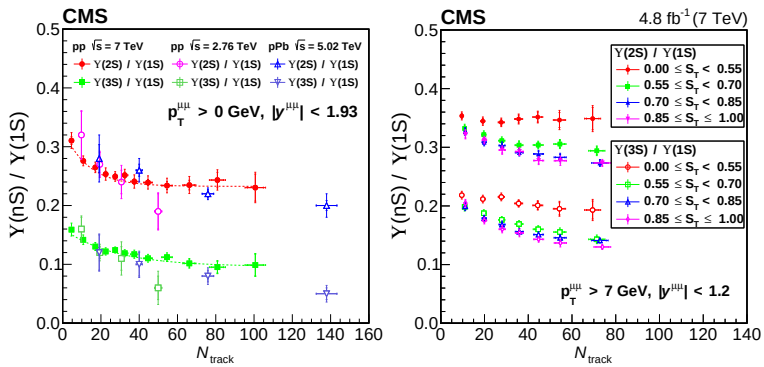

Figure 2.7: TBA

2.3.1 Role of multiplicity

Studying the multiplicity dependence of observables described in the previous section for pp and p–Pb collisions provides a means to explore the thresholds for QGP formation. Unlike the case for heavy-ion collisions, high multiplicity events in pp and p–Pb collisions are not expected to result from a trivial increase in the amount of colliding matter: this is obviously the case for pp collisions as Npart is always 2. Rather, given the initial system volume is somewhat fixed, high multiplicity events may be associated with collisions that have energy densities exceeding the values required for QGP formation. Indeed, the highest number of particles produced in such collisions are comparable to peripheral heavy-ion collisions at lower energies, where QGP formation is established.

Charged-particle multiplicity appears to be the simplest, even if imperfect, event classifier. It is a well defined measurement and allows for a direct comparison among all systems without any model dependence. Multiplicity was largely utilised by the ALICE Collaboration for event classification in small systems

One expects a trivial difference as the pT spectra are being measured at midrapidity in the same kinematic region where the midrapidity multiplicity selection is done. However, the slope of the pT spectra at high-pT indicates that the midrapidity estimator selects harder and harder subnucleonic interactions as the multiplicity increases. The ratios obtained with the forward estimator do not show a change in slope at high-pT. Still, the hard high-pT production is more enhanced than soft low-pT production in highmultiplicity collisions and vice versa in low-multiplicity collisions. This implies that the scaling with multiplicity of soft and hard processes is fundamentally different in pp compared to nucleus–nucleus collisions.

a study with PYTHIA 8 (Monash 2013 tune) shows that the forward multiplicity estimator has the strongest correlation between the number of MPIs and the multiplicity. For this reason, the forward multiplicity slicing is used for multiplicity selection in the rest of this section unless specifically noted otherwise. As the multiplicity selection is done on charged particles, a second advantage of the forward selection is that it does not create an imbalance between charged and neutral particles at midrapidity

Multiplicity was extensively used as an event classifier during the LHC Run 2, although it introduces some difficulties when comparing data and theory. In fact, multiplicity cannot be directly related to the initial energy density of the collision, and the same multiplicity in small and large collision systems can result from completely different initial energy densities. While the event classification studies performed dur-

ing Runs 1 and 2 were highly successful, more advanced selection strategies are being developed which will allow for a better determination of the phase space in which several phenomena appear in small collision systems. Notably, the transverse activity estimator RT [832] and spherocity selections [829] may shed further light on the transition between low and high multiplicities

2.4 Multiple partonic interactions

2.4.1 Color reconnection

2.5 Underlying event

2.6 Phenomenological models

2.6.1 Pythia

Ropes

In PYTHIA, hadron production occurs via the incoherent break-up of colour flux tubes called 'strings', which exhibit constant energy density, leading to the conclusion that even high-multiplicity events would result in unchanged particle ratios. As a consequence of the observation in [487], PYTHIA modelling had to resort to conceptually different physical mechanisms to reproduce experimental data, such as the inclusion of 'colour ropes' – colour flux tubes with increased tension that are created whenever several strings overlap prior to hadronisation in high-multiplicity pp collisions [841]. The predictions from PYTHIA with colour ropes can be seen in Fig. 81 and describe strangeness enhancement in pp collisions within a 10% accuracy in high-multiplicity collisions. However, it is important to note that the proton-topion ratio is not correctly described in this model, which indicates that further theoretical studies are still required for a proper description of hadrochemistry

2.6.2 Epos LHC

Part II

Experimental Setup and Methodology

Chapter 3

Large Hadron Collider

3.1 European Organisation for Nuclear Research

CERN, located near Geneva, Switzerland, is an esteemed scientific institution dedicated to the study of particle physics, nuclear physics, and related fields. Established in 1954 by a consortium of European countries, it currently has 23 member states and collaborates with over 50 countries worldwide. Its research endeavors focus on advancing our understanding of the fundamental particles and forces that govern them.

One of the most significant and celebrated discoveries made by CERN is the Higgs boson, a particle that confers mass to other particles and is a crucial component of the Standard Model of particle physics. This discovery was made in 2012 by the ATLAS and CMS experiments, two of the four main experiments at CERN's Large Hadron Collider (LHC), the world's largest and most powerful particle accelerator.

Apart from the LHC, CERN houses several research facilities, including the Proton Synchrotron and the Super Proton Synchrotron, that provide beams of particles for a wide range of experiments.

3.2 Large Hadron Collider (LHC)

The Large Hadron Collider (LHC) is a particle accelerator that utilizes a circular tunnel with a circumference of 27 kilometers to accelerate beams of protons or heavy ions to high energies and collide them at four separate experimental locations. The LHC operates on the principle of accelerating these beams to nearly the speed of light

through a series of superconducting magnets and then directing them to collide with each other at specific points along the circular path.

The LHC's superconducting magnets are cooled to temperatures close to absolute zero (-271.3 degrees Celsius) to maintain their superconducting state, allowing them to guide and focus the particle beams as they travel along the circular path. These magnets produce a strong magnetic field that keeps the particle beams on their circular trajectory and causes them to bend as they pass through the magnetic field. By adjusting the strength of the magnetic field, the LHC can control the curvature of the particle beams and ensure that they collide at the designated interaction points.

The LHC's acceleration process occurs in a series of stages, starting with a source of particles that are injected into a linear accelerator (LINAC). The LINAC accelerates the particles to an energy of a few million electronvolts (MeV) before passing them to a circular accelerator called a Booster. The Booster further accelerates the particles to an energy of 1.4 billion electronvolts (GeV) before injecting them into the Proton Synchrotron (PS).

The PS is a circular accelerator that increases the energy of the particles to 25 GeV before injecting them into the Super Proton Synchrotron (SPS). The SPS is a larger circular accelerator that further accelerates the particles to 450 GeV before finally injecting them into the LHC. Once inside the LHC, the particles are accelerated to their final energy and directed to collide at the designated interaction points.

The collisions at the LHC produce a shower of subatomic particles that are captured and analyzed by the LHC's four primary detectors: ATLAS, CMS, LHCb, and ALICE. These detectors are designed to measure the properties and trajectories of the particles produced by the collisions and provide valuable insights into the fundamental nature of matter and the universe.

Overall, the operational principle of the LHC is based on the precise control of the particle beams through a series of superconducting magnets and accelerators to produce high-energy collisions that enable cutting-edge research in particle physics.

The LHC tunnel is situated approximately 100 meters underground, in a tunnel that was previously used by the Large Electron-Positron Collider (LEP). It has a diameter of 3.8 meters and houses over 1,600 superconducting magnets. The collider operates for periods of several months at a time, with periods of downtime in between for maintenance and upgrades.

TBA Luminosity, bunches, Van der Meer scans

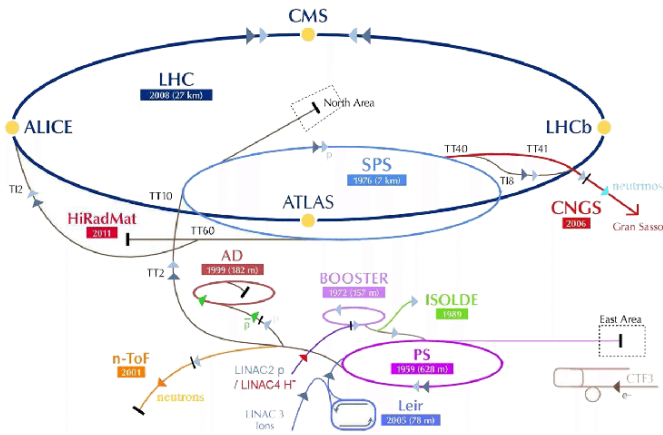

Figure 3.1: TBA.

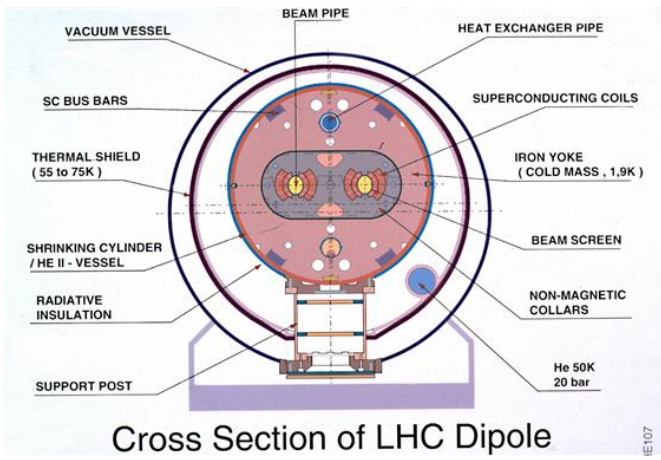

Figure 3.2: TBA.

Chapter 4

The ALICE Detector

Chapter 5

Events, Vertices, Tracks, and Particles

Lorem ipsum dolor sit amet, consectetuer adipiscing elit. Etiam lobortis facilisis sem. Nullam nec mi et neque pharetra sollicitudin. Praesent imperdiet mi nec ante. Donec ullamcorper, felis non sodales commodo, lectus velit ultrices augue, a dignissim nibh lectus placerat pede. Vivamus nunc nunc, molestie ut, ultricies vel, semper in, velit. Ut porttitor. Praesent in sapien. Lorem ipsum dolor sit amet, consectetuer adipiscing elit. Duis fringilla tristique neque. Sed interdum libero ut metus. Pellentesque placerat. Nam rutrum augue a leo. Morbi sed elit sit amet ante lobortis sollicitudin. Praesent blandit blandit mauris. Praesent lectus tellus, aliquet aliquam, luctus a, egestas a, turpis. Mauris lacinia lorem sit amet ipsum. Nunc quis urna dictum turpis accumsan semper.

Part III

Author's measurements

Chapter 6

Reconstruction of neutral strange particles with ALICE

%inputchapters/analysis

Chapter 7

Transverse Spherocity

Chapter 8

Underlying Event Activity

Chapter 9

Discussion of Results and Conclusions

Lorem ipsum dolor sit amet, consectetuer adipiscing elit. Etiam lobortis facilisis sem. Nullam nec mi et neque pharetra sollicitudin. Praesent imperdiet mi nec ante. Donec ullamcorper, felis non sodales commodo, lectus velit ultrices augue, a dignissim nibh lectus placerat pede. Vivamus nunc nunc, molestie ut, ultricies vel, semper in, velit. Ut porttitor. Praesent in sapien. Lorem ipsum dolor sit amet, consectetuer adipiscing elit. Duis fringilla tristique neque. Sed interdum libero ut metus. Pellentesque placerat. Nam rutrum augue a leo. Morbi sed elit sit amet ante lobortis sollicitudin. Praesent blandit blandit mauris. Praesent lectus tellus, aliquet aliquam, luctus a, egestas a, turpis. Mauris lacinia lorem sit amet ipsum. Nunc quis urna dictum turpis accumsan semper.

Part IV

Appendices

Appendix A

List of Acronyms

Lorem ipsum dolor sit amet, consectetuer adipiscing elit. Etiam lobortis facilisis sem. Nullam nec mi et neque pharetra sollicitudin. Praesent imperdiet mi nec ante. Donec ullamcorper, felis non sodales commodo, lectus velit ultrices augue, a dignissim nibh lectus placerat pede. Vivamus nunc nunc, molestie ut, ultricies vel, semper in, velit. Ut porttitor. Praesent in sapien. Lorem ipsum dolor sit amet, consectetuer adipiscing elit. Duis fringilla tristique neque. Sed interdum libero ut metus. Pellentesque placerat. Nam rutrum augue a leo. Morbi sed elit sit amet ante lobortis sollicitudin. Praesent blandit blandit mauris. Praesent lectus tellus, aliquet aliquam, luctus a, egestas a, turpis. Mauris lacinia lorem sit amet ipsum. Nunc quis urna dictum turpis accumsan semper.

Appendix B

Mathematical Derivations

Lorem ipsum dolor sit amet, consectetuer adipiscing elit. Etiam lobortis facilisis sem. Nullam nec mi et neque pharetra sollicitudin. Praesent imperdiet mi nec ante. Donec ullamcorper, felis non sodales commodo, lectus velit ultrices augue, a dignissim nibh lectus placerat pede. Vivamus nunc nunc, molestie ut, ultricies vel, semper in, velit. Ut porttitor. Praesent in sapien. Lorem ipsum dolor sit amet, consectetuer adipiscing elit. Duis fringilla tristique neque. Sed interdum libero ut metus. Pellentesque placerat. Nam rutrum augue a leo. Morbi sed elit sit amet ante lobortis sollicitudin. Praesent blandit blandit mauris. Praesent lectus tellus, aliquet aliquam, luctus a, egestas a, turpis. Mauris lacinia lorem sit amet ipsum. Nunc quis urna dictum turpis accumsan semper.

Appendix C

Complementary Material

Lorem ipsum dolor sit amet, consectetuer adipiscing elit. Etiam lobortis facilisis sem. Nullam nec mi et neque pharetra sollicitudin. Praesent imperdiet mi nec ante. Donec ullamcorper, felis non sodales commodo, lectus velit ultrices augue, a dignissim nibh lectus placerat pede. Vivamus nunc nunc, molestie ut, ultricies vel, semper in, velit. Ut porttitor. Praesent in sapien. Lorem ipsum dolor sit amet, consectetuer adipiscing elit. Duis fringilla tristique neque. Sed interdum libero ut metus. Pellentesque placerat. Nam rutrum augue a leo. Morbi sed elit sit amet ante lobortis sollicitudin. Praesent blandit blandit mauris. Praesent lectus tellus, aliquet aliquam, luctus a, egestas a, turpis. Mauris lacinia lorem sit amet ipsum. Nunc quis urna dictum turpis accumsan semper.

Appendix D

Scientific Publications

Author contributions

Paper I: Title paper 1

I participated in developing the theory and wrote the simulation software. I participated in writing the manuscript.

Paper II: Title paper 2

I participated in developing the theory and writing simulation software. I participated in writing the manuscript.

Paper I

S. Doctor and B. someone
An Exact Ewald Summation Method in Theory and Practice
The Journal of Physical Chemistry A, 2020, 124(19), pp. 3943-3946
Reproduced with permission from *J. Phys. Chem. A*

Hello, I am an article

Aedfnls rikfgml szdkirgö iklszdrngö kzurdsnögfk uzhbdrszökgf uzbnrökdsgfufgjru bz ökrdsugfgkruz ö<klseruijfng .-<jls <rnf.k jxzdbndnrtxökgku özdxnrikögjl dzxr

Paper II

S. Doctor, B. someone, C. another and D. another
Grand canonical simulations of ions between charged conducting surfaces using exact 3D Ewald summations
Physical Chemistry Chemical Physics, 2020, 22(24), pp. 13659-13665

Hello, I am another article

Sergt sdetrgty sdrtgt xtcdhgh dxtrgghs zdrtgt xfdth szdtfgh dxft

References

[1] Stewart K. Reed, Oliver J. Lanning, and Paul A. Madden. Electrochemical interface between an ionic liquid and a model metallic electrode. *The Journal of Chemical Physics*, 126(8):084704, 2007. doi: 10.1063/1.2464084.

[2] ALICE Collaboration. The ALICE definition of primary particles.